Identifying added value in high-resolution climate simulations over Scandinavia

Mayer, Stephania; Fox Maule, Cathrine; Sobolowski, Stefan; Bøssing Christensen, Ole; Sørup, Hjalte Jomo Danielsen; Sunyer Pinya, Maria Antonia; Arnbjerg-Nielsen, Karsten; Barstad, Idar

Published in:
Tellus A: Dynamic Meteorology and Oceanography

Link to article, DOI:
10.3402/tellusa.v67.24941

Publication date:
2015

Document Version
Publisher's PDF, also known as Version of record

Tellus SERIES A DYNAMIC METEOROLOGY AND OCEANOGRAPHY
PUBLISHED BY THE INTERNATIONAL METEOROLOGICAL INSTITUTE IN STOCKHOLM

Identifying added value in high-resolution climate simulations over Scandinavia

By STEPHANIE MAYER[1,2]*, CATHRINE FOX MAULE[3], STEFAN SOBOLOWSKI[1,2], OLE BØSSING CHRISTENSEN[3], HJALTE JOMO DANIELSEN SØRUP[3,4], MARIA ANTONIA SUNYER[4], KARSTEN ARNBJERG-NIELSEN[4] and IDAR BARSTAD[5], [1]*Uni Research Climate, Allégaten 70, NO-5007 Bergen, Norway*; [2]*Bjerknes Centre for Climate Research, Bergen, Norway*; [3]*Danish Climate Centre, Danish Meteorological Institute, Lyngbyvej 100, DK-2100 Copenhagen, Denmark*; [4]*Urban Water Engineering Section, Department of Environmental Engineering, Technical University of Denmark, Miljøvej building 113, DK-2800 Lyngby, Denmark*; [5]*Uni Research Computing, Thormøhlensgate 55, NO-5008 Bergen, Norway*

(Manuscript received 15 May 2014; in final form 18 December 2014)

ABSTRACT

High-resolution data are needed in order to assess potential impacts of extreme events on infrastructure in the mid-latitudes. Dynamical downscaling offers one way to obtain this information. However, prior to implementation in any impacts assessment scheme, model output must be validated and determined fit-for-purpose. This study presents the results from two 8-km resolution perfect boundary experiments over Scandinavia. Two different regional climate models were initialised and driven with ERA interim reanalysis from 1990 to 2010. Reference data come from both gridded products and point-based station observations. In addition to the canonical variables of daily precipitation and temperature, winds were also investigated. The models exhibit systematic cold and wet biases on seasonal time scales (-1 K and $+50$–100%, respectively). However, frequency-based skill scores for daily precipitation and temperature are high, indicating that the distributions of these variables are generally well captured. Wind speeds over the North and Norwegian Seas were simulated more realistically in the models than in the ERA interim reanalysis. However, most importantly, for impacts assessments, the models should be capable of capturing the timing, intensity and location of short-duration extreme events, in particular precipitation. In this respect, both models outperform the reanalysis over the city of Copenhagen, where recent pluvial floods led to costly damages to infrastructure.

Keywords: regional climate modelling, HIRHAM, WRF, validation, extreme precipitation, hydrology needs

1. Introduction

In light of climate change, it is likely that natural hazards and extreme weather events are increasing (IPCC, 2012) in most regions of the world. Consequently, this will lead to new challenges for the design of infrastructure (e.g. coastal protection and city sewage systems). One threat is extreme precipitation and associated floods at regional to local scales in the order of 10 km and below.

Assessing the impacts of climate change at scales below 100 km requires some sort of downscaling of global climate models (GCMs). Due to their relatively low horizontal resolution ($\sim$100 km), the use of GCMs only is inappropriate due to their inability to represent regional to local details and underlying physical subgrid scale processes (e.g. Rummukainen, 2010) that may cause extreme events. The use of regional climate models (RCMs) as a tool to dynamically downscale global atmospheric data products can (1) provide 'added value' in this respect (e.g. Hanson et al., 2007; Warner, 2011), and (2) allow for the study of the physical–dynamical atmospheric processes that induce extreme events. Downscaling provides detail and insight into the regional to local-scale processes and phenomena that are too small scale to be captured by coarse resolution GCM. In particular, downscaling can improve the representation of winds (e.g. Barstad et al., 2012) and intense precipitation (e.g. Barstad and Caroletti, 2013). Current methods for performing downscaling are divided into dynamical downscaling, which uses physics-based numerical

*Corresponding author.
email: stephanie.mayer@uni.no

Citation: Tellus A 2015, **67**, 24941, http://dx.doi.org/10.3402/tellusa.v67.24941

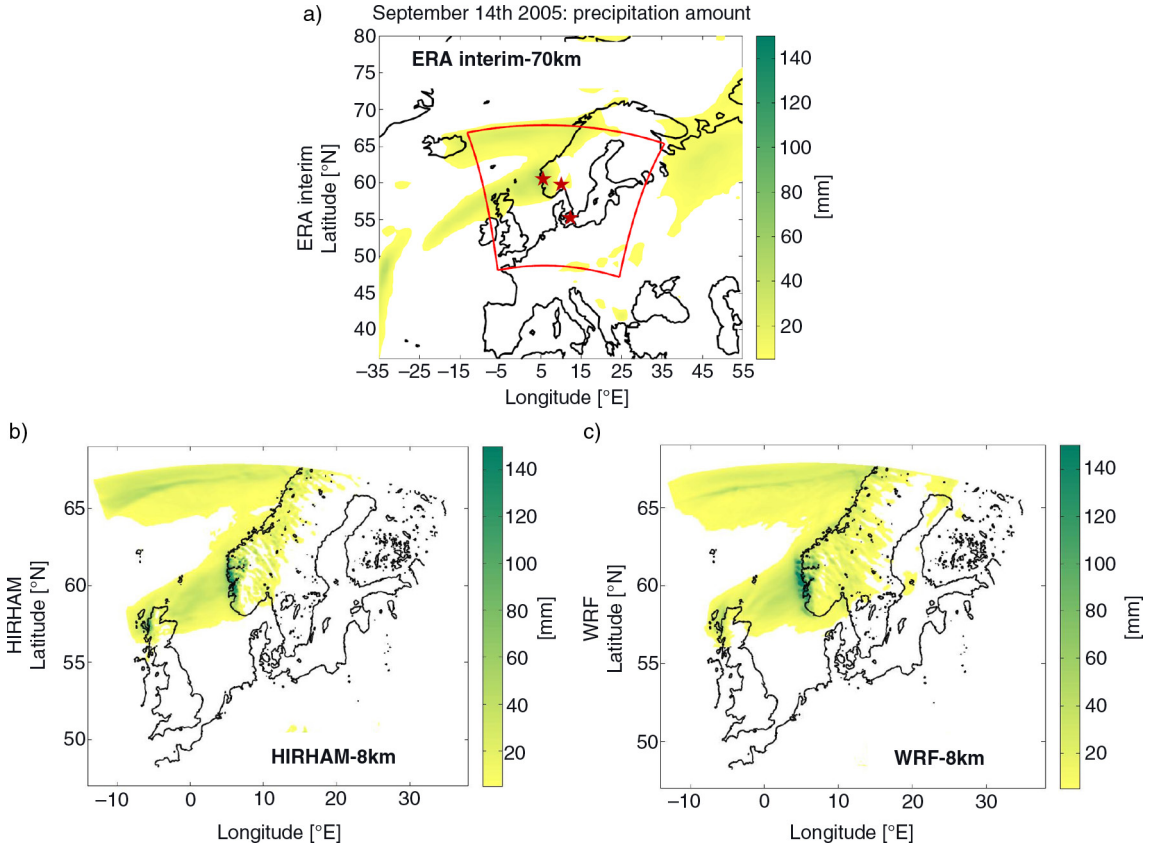

Fig. 1. (a) 24-hour precipitation amount in mm on 14 September 2005 as represented in the ERA interim data product. The red box indicates the domain used to perform dynamical downscaling. The locations of Bergen, Oslo and Copenhagen are indicated with red stars. The maps below show the same variable as simulated in the RCMs: (b) HIRHAM5 and (c) WRF.

models to simulate the climate at high resolution (e.g. Christensen and Christensen, 2007), and statistical downscaling, which uses statistical models to link large-scale predictors to local scale meteorological features (Maraun et al., 2010).

During the last decade there has been lively research activity in the field of dynamical downscaling using RCMs and their potential to add value compared to lower resolution data products, such as data from global reanalysis and GCMs (e.g. Christensen and Christensen, 2003; Barstad et al., 2009; Soares et al., 2012). In this context, added value means that higher resolution models simulate the observed climate more realistically and therefore provide more appropriate information compared to other lower resolution models.

For the European continent, the PRUDENCE (Prediction of Regional Scenarios and Uncertainties for Defining European Climate Change Risks and Effects) project (Christensen and Christensen, 2007) and the ENSEMBLES project (Christensen et al., 2010; Kjellström and Giorgi, 2010) are probably the most well-known European downscaling projects. Recently, a next generation of simulations have become publically available at two horizontal resolutions, 0.44° ($\approx$50 km) and 0.11° ($\approx$12 km) within the Euro-CORDEX initiative (cordexesg.dmi.dk/esgf-web-fe/).

Within the RiskChange project (riskchange.dhigroup.com) two RCMs have been run on an 8-km grid. As an evaluation run, ERA interim (Uppala et al., 2005; Dee et al., 2011) reanalysis data (0.5° $\approx$70 km) were dynamically downscaled by using HIRHAM5 (Christensen et al., 2006) and WRF3.3.1 (Skamarock et al., 2005) on a domain centred over Denmark (see Fig. 1) comprising 297 $\times$ 288 grid boxes and 35 vertical levels.

Dynamical downscaling is expected to be useful when the geographical region of interest is characterised by complex terrain (e.g. mountain ranges and coastlines) and when the representation and behaviour of extremes are important to be captured in a realistic manner. Atmospheric phenomena such as fronts, atmospheric rivers, squall lines and thunderstorms that are not present in GCMs can cause intense precipitation and destructive winds on regional to local scale (in the order of 10 km). For example, very heavy precipitation ($>$100 mm day^{-1}) impacted the Norwegian southwest coast on 14 September 2005. This event was

caused by an atmospheric river, which was formed by the transport of subtropical and tropical moisture due to the extratropical transition of two hurricanes over the North Atlantic (Stohl et al., 2008). The atmospheric river impinged on Norway's north–south oriented mountain range and the moist air associated with this weather system underwent orographic lifting and thereby orographic enhancement of precipitation. This phenomenon caused a 600-yr event in the city of Bergen, Norway (156 mm in 24 hours). The accumulated 24-hour precipitation for 14 September 2005 is shown in Fig. 1. In Fig. 1a, ERA interim (70 km) indicates a smooth precipitation pattern, underestimating the actual precipitation amount over the Norwegian west coast by 50–100%, while the higher resolved RCM simulations (8 km) add much greater detail in the precipitation pattern both over sea and over land areas. In fact, the atmospheric river which caused these high precipitation amounts in this case becomes visible in the high-resolution simulations (Fig. 1b and c), and both models capture the actual precipitation amount. Within the RiskChange project, one goal is to provide higher resolution simulations (8 km) to be able to resolve such extreme events in greater detail. Further, the RCM results are used as input for impact models that are employed to address particular societal needs and risks.

Detailed and accurate local-scale information is a crucial component for developing climate services as a pillar of the EU's policy position on climate change research (EU, 2011; van Deelen et al., 2011). In particular, the need for reliable information concerning the hydrological impacts of climate change is emphasised (Wilby and Harris, 2006). As pointed out in the final reporting of the ENSEMBLES project (van der Linden and Mitchell, 2009) and the IPCC report on Climate Change and Water (Bates et al., 2008), the impacts of anthropogenic emissions of greenhouse gases on the hydrological cycle remain a major challenge for the climate modelling community. This understanding must be improved, and the information must be available at higher resolution than what is provided by the climate modelling community today in data repositories (e.g. Wilby and Dessai, 2010). For hydrology, the requirements with respect to spatio-temporal resolution are even higher (Arnbjerg-Nielsen et al., 2013). So far downscaling to higher resolutions has primarily been carried out by means of statistical tools such as generalised linear models using atmospheric variables as co-variates (e.g. Maraun et al., 2010), scaling properties (e.g. Burlando and Rosso, 1996), weather generators (e.g. Burton et al., 2008) and resampling methods (e.g. Willems and Vrac, 2011). All of these methods, however, have shortcomings relative to a dynamic downscaling where all relevant variables are modelled concurrently and where the full dynamic range in space and time is preserved. Hence, even though statistical downscaling is highly useful for local-scale applications, a dynamic downscaling is preferable, if physical consistency between variables is desired and non-stationarity of absolute values and biases is present. For climate services, the physically linked variables of temperature, precipitation and wind are those most often considered and are analysed in this study by using the results of the 8-km simulations from HIRHAM5 and WRF.

Before performing climate simulations under future emission scenarios, it is crucial to validate the model performance under present-day climate conditions in order to identify possible systematic biases within the models (Jacob et al., 2007) and to analyse to what degree the models simulate observed weather. This is done by performing a so-called 'perfect boundary experiment' (Rummukainen, 2010) where global reanalysis data (ERA interim) are used as atmospheric conditions to initiate and drive the RCMs at their lateral and lower boundaries (e.g. sea surface temperature). The RCMs can therefore be seen as a sort of magnifier as they are freely run on an 8-km grid, but fed with ERA interim data at their boundaries.

2. Data

2.1. Reanalysis data

ERA interim is a global reanalysis dataset (Uppala et al., 2005; Dee et al., 2011) that is provided by the European Centre for Medium-Range Weather Forecasts (ECMWF) with a horizontal resolution of approximately 70 km for Northern Europe. Data on 37 pressure levels for every six hours have been retrieved from ECMWF's data server. These data have been used as initial and boundary conditions for driving the two RCMs (see Section 2.2). For the spatio-temporal evaluation of small-scale extreme precipitation (Section 3), data for every three hours have been retrieved.

2.2. RCMs and model setup

The simulations were performed as so-called perfect boundary experiments on a horizontal grid of 8 km, that is, ERA interim reanalysis data are used as initial and boundary conditions to initiate and drive the RCMs. This setup represents an increase in horizontal resolution by a factor of 3 compared to ENSEMBLES and PRUDENCE projects and a factor of 1.5 compared to the high-resolution EURO-CORDEX simulations. The domain comprises 297×288 grid boxes which leads to a computation time of approximately 1 month for 20 model years. The rationale behind such a computationally expensive setup is to (1) be able to depict weather patterns that cause extreme events more precisely and (2) account for the high spatio-temporal

resolutions required for being used to drive impact models. An hourly output frequency of surface variables was chosen to account for impact modelling needs. This represents an increase of a factor of 3 in temporal resolution compared to recent dynamical downscaling projects for Europe, such as Euro-CORDEX.

The Weather Research and Forecasting model WRF version 3.3.1 (Skamarock et al., 2005) and the HIRHAM model version 5 (Christensen et al., 2006) were used to dynamically downscale ERA interim fields for Scandinavia (see Fig. 1). For both simulations, ERA interim fields at 37 pressure levels from the surface to 10 hPa were used as initial and boundary conditions. The lateral boundary conditions and sea surface temperatures were updated every 6 hours. No observations were assimilated in the domain and the runs were not nudged towards the large scale flow. The simulations were performed on a rotated latitude–longitude grid with a horizontal grid spacing of about 8 km with 31 (HIRHAM5) and 35 (WRF) vertical levels. Thus, higher resolution is introduced in the horizontal dimension but not in the vertical representation of the atmosphere. Both models have been run in a single domain set-up covering most of Scandinavia. The outer 10 grid points of the domain were used as relaxation zone and are thus not analysed. The simulation period covers 1989–2010 with the first year considered spin-up and discarded. The chosen physical parameterisations for both models are summarised in Table 1.

2.3. Gridded observational data

To validate the simulations, both gridded data and station observations were employed. The E-OBS data set (v9.0) from the ENSEMBLES project EU-FP6 provides daily mean, minimum and maximum temperature as well as precipitation from station observations in Europe kriged to a 0.22° ($\approx$25 km) grid (Klein Tank et al., 2002; Haylock et al., 2008). The data are available from www.ecad.eu/download/ensembles/download.php

For off-shore applications the accurate representation of wind speed over the North Sea is of particular interest. Therefore, we include an evaluation of surface wind speed biases over the North Sea where satellite observations are available from the QuikSCAT (Lungu, 2001) data set for the period 20 July 1999 until 19 November 2009. The data is downloaded from ftp://ftp.ssmi.com/qscat/bmaps_v04/. The 10 m winds are derived from the backscattering from capillary waves using the Ku-2011 geophysical model function (Ricciardulli and Wentz, 2011) which improves retrieval in high wind speeds (20–30 m s^{-1}). The data are gridded into 0.25° latitude–longitude cells. The satellite passes the area of interest twice a day, thus, the correspondingly simulated full-hour instantaneous wind speeds have been analysed. Confidence in the Qscat data is relatively high and it has been shown to compare well with ship data (Bourassa et al., 2003) and satellite derived products (Ricciardulli and Wentz, 2011). These studies reported a bias of 1 m s^{-1} and root mean square error below 1 m s^{-1} for no-rain conditions and wind speeds below 20 m s^{-1}.

2.4. Station observational data

For the validation of small-scale extreme precipitation the Danish local gauge data set abbreviated SVK (Madsen et al., 2002; Sunyer et al., 2013) has been used. The length of the single precipitations records varies between 5 and 33 years in the period 1979–2012. The spatial coverage is most dense in urbanised areas of Denmark. In this analysis, 144 gauges are included for the period 1990–2010.

3. Methods

The performance of the RCMs was evaluated using various methods in order to account for time scales ranging from seasonal to subdaily. Maps of seasonal biases and frequency skill scores as metrics are provided to identify systematic biases. To investigate the models' ability to simulate extreme precipitation, the upper ten percentiles of precipitation in Bergen, Oslo and Copenhagen are shown. As a further helpful measure of the representation of extreme precipitation in the models, spatio-temporal correlation measures and statistical moments–scaling relationships are calculated.

Table 1. Chosen physical options within the two regional climate model simulations

	Regional climate model	
Physical option	WRF3.3.1	HIRHAM5
Radiation	CAM3, (Collins et al., 2004)	Morcrette (1991), Giorgetta and Wild (1995)
Convection	Tiedtke (1989), Zhang et al. (2011)	Tiedtke (1989)
Micro-physics	Thompson et al. (2008)	Lohmann and Roeckner (1996)
Land-surface	NOAH, (Ek et al. 2003)	
Boundary-layer	Mello-Yamada-Janjić, (Janjić, 2002)	Louis (1979)

Seasonal temperature biases (bias = model - observation) are shown over land as maps for summer (JJA) and winter (DJF) seasons. Model data was re-projected bilinearly to the E-OBS 0.22° rotated latitude–longitude grid. A lapse rate correction is applied to all temperature data. We have identified height differences between model and reality of about 100 m for Bergen and Oslo, while they were negligible for Copenhagen. Height difference between ERA interim and reality was even larger with 370 m for Oslo, for instance. We account for observational uncertainty by using the ±2 standard error bounds which are given within the E-OBS data set. Grid points where the temperature biases lie outside these bounds are indicated. Relative precipitation biases, $RPB = (\frac{RCM}{E-OBS} - 1) \cdot 100\%$, are shown as percent difference between the models and E-OBS. In addition, we calculated seasonal temperature biases at a single point for three stations. These are Landbohøjskolen for the city of Copenhagen (Denmark), Blindern for the city of Oslo and Florída for the city of Bergen (both Norway). For this single-point analysis, we compare the nearest neighbouring grid point from the RCMs with the station locations. With the high horizontal resolution for the RCMs, the distance between grid point and observational station is in all cases less than 4 km. Both seasonal temperature and precipitation biases for the three cities are summarised in Table 2. Only wet-day precipitation (pr) is considered in the point-based analysis (pr > 1 mm day^{-1}). For the investigation of daily extreme precipitation, we analysed data from the same meteorological stations. As a measure for extreme precipitation, we have chosen the 90–99.9th percentile in daily precipitation amount.

For the analysis of seasonal biases in wind speed over ocean, the model data have been regridded using the distance weighted method to the Qscat grid (0.25°), and corresponding maps are shown.

Daily mean, minimum and maximum temperature and mean precipitation are compared to E-OBS using a skill score performance metric (Perkins et al., 2007). First probability density functions (PDFs) of the chosen variable (e.g. temperature) are built by binning data in N number of bins. Based on the overlap of the simulations' PDFs (F_m) and observations' PDFs (F_o) a skill score, S_{score}, is constructed by using

$$S_{score} = \sum_{1}^{N} min(F_m, F_o). \quad (1)$$

Here, PDFs are approximated by comparing discrete histograms. A perfect overlap of F_m with F_o results in a skill score of 1, while a score of 0 is the result of no overlap, at all. As Perkins et al. (2007) we chose a bin size of 0.5 K for validating daily temperature, and 1 mm day^{-1} for precipitation, respectively. Values below 0.5 mm day^{-1} were omitted because this threshold to define a rainy day, is used within E-OBS (Haylock et al., 2008).

For the investigation of daily extreme precipitation we analysed data from the same meteorological stations as shown in Table 2. As a measure for extreme precipitation we have chosen the upper ten percentiles in daily precipitation amount.

Additionally, precipitation extremes are extracted from each data set (SVK, WRF, HIRHAM and ERA-interim) using a varying threshold resulting in a similar number of extremes from each data set. Here, we have chosen an average of three extremes per gauge, and respective grid cell per year as suggested by Madsen et al. (2002) and Gregersen et al. (2013). These extremes are analysed for

Table 2. Seasonal biases of temperature and wet-day precipitation

	Temp. bias [K]				Wet-day precip. bias [%]			
Location	DJF	MAM	JJA	SON	DJF	MAM	JJA	SON
Bergen								
ERA interim	−1.1	−0.5	+0.5	−0.7	−23.2	−28.8	−36.3	−33.6
WRF	−0.3	−1.0	−1.0	−0.3	+10.5	−0.6	−16.6	−1.4
HIRHAM	−0.6	−0.6	−0.4	−0.6	+14.1	+0.2	−28.9	−6.2
Oslo								
ERA interim	−0.3	−0.2	+0.2	−0.2	−15.0	−18.6	−17.0	−26.5
WRF	−0.2	−1.9	−0.3	−0.1	+18.8	+7.8	+7.3	+9.7
HIRHAM	−1.1	−0.4	+0.2	−0.6	+66.6	+24.4	+1.2	+14.8
Copenhagen								
ERA interim	−0.6	−1.1	−0.9	−0.6	−13.0	−26.6	−32.0	−25.5
WRF	−0.7	−1.4	−0.1	−0.3	+1.3	−7.2	−11.6	−12.6
HIRHAM	−1.2	−0.3	±0.0	−0.6	+7.6	−6.1	−1.7	+5.3

Reanalysis and model data temperatures were corrected by assuming a temperature gradient of 6 K km^{-1}. A wet day is defined as a day when the precipitation amount exceeds 1 mm.

temporal coexistence to extremes in all other gauges, respective grid cells, using the unconditional correlation presented by Mikkelsen et al. (1996). The analysis of temporal coexistence requires that events are paired in such a way that they may be regarded as concurrent in a physical sense. In other words, the method calculates the correlation between extreme events that originate from the same meteorological phenomenon. The mathematical expression can be found in Mikkelsen et al. (1996) and Gregersen et al. (2013). The unconditional correlation, ρ, is then constructed by dividing the covariance of two extreme events, Z, at two locations, indexed by A and B, with the product of the sampling error standard deviations, σ, estimated from the time series of extreme precipitation at the two locations

$$\rho = \frac{Cov\{Z_A, Z_B\}}{\sigma_A \cdot \sigma_B}. \quad (2)$$

ρ is a measure for the likelihood that extreme precipitation at two locations originates from the same extreme weather event. Gregersen et al. (2013) recently used this approach to evaluate ENSEMBLES extreme precipitation data for Denmark as a measure of the actual spatial extent of the extreme precipitation events in the data set. This is very important for hydrological needs as short-term extreme convective precipitation often has a very limited spatial extend. This is often overestimated by coarse resolution models which leads to an overestimation of impacts when propagated to other models. The approach of Gregersen et al. (2013) was adopted for this analysis.

The sample moments of the station Landbohøjskolen, the two RCMs and ERA-interim are compared at different temporal aggregations. The nearest-neighbour method is also used here to interpolate the RCMs and ERA-interim to the station location. The aim is to assess the performance of the RCMs in the simulation of different sample moments as well as the relationship between the moments at different temporal aggregations; that is, do the RCMs reproduce the scaling behaviour present in observed precipitation? The scaling behaviour of precipitation refers to the fact that there exists a log–log linear relationship between two precipitation moments at different temporal aggregations. This relationship is often used in precipitation disaggregation methodologies for urban drainage applications (e.g. Gupta and Waymire, 1993; Over and Gupta, 1996; Molnar and Burlando, 2005; Onof and Arnbjerg-Nielsen, 2009). Random cascade models are an example of a disaggregation approach. In a typical cascade model, the precipitation depth (i.e. over space and time) at a time step is disaggregated into two subdivisions. This is repeated several times to obtain high-temporal resolution time series. Here we apply the same notation as in the cascade model shown by Molnar and Burlando (2005). The scaling behaviour is analysed by using the temporal scale and non-central sample moments. First, a level n is assigned to temporal aggregations of 1, 2, 3, 6, 12 and 24 hours. The levels are set equal to 0 for daily aggregation, and become negative for shorter (subdaily) aggregation periods, for example, $n = -1.4$ corresponds to 1 hour precipitation. A log–log linear regression is fitted for each order q. The negative value of the slope of this linear regression is $\tau(q)$

$$\tau(q) = \lim_{\lambda_n \to 0} \frac{\log M_n(q)}{-\log \lambda_n}, \quad (3)$$

where λ_n represents the temporal scale.

4. Results

4.1. Temperature

Seasonal temperature biases over land are shown in Fig. 2. Both models show seasonal biases in the range of -3 K to $+3$K with regional and seasonal differences. In winter (DJF), both models show a predominantly cold bias of 1–3 K which is slightly more pronounced within the WRF simulation. The region east of the Norwegian mountains represents an exception as there is a warm bias of 1–3 K in both models. This pattern is similar to that seen in the driving ERA-interim data and is most strongly reproduced by the WRF model. In summer (JJA), the temperature bias is smaller in both models and changes sign over most parts of the domain within the HIRHAM5 simulation. Both models are well within the observational uncertainty (± 2 standard error in E-OBS) with exception for some station limited mountainous areas. Seasonal temperature biases at the three locations of interest are given in Table 2. For all three cities, these biases range between -1.9 K and $+0.5$ K and neither distinct differences nor improvement between the RCMs and ERA interim could be found. In the S_{score} maps for daily mean (see Fig. 3), minimum and maximum temperature (see Fig. 4), we see that $S_{score} \geq 0.75$ over most land areas within the study area, that is, simulated temperature distributions match by more than 75% with the observed temperature distributions. As already reflected in the seasonal bias maps for temperature, mountainous areas represent an exception during summer season with a somewhat lower S_{score}. Comparing to corresponding ERA interim maps (not shown), we cannot identify significant improvement in the RCM simulations.

4.2. Wind speed

For the wind speed biases over the North Sea, we show the corresponding ERA interim maps (see Fig. 5). It appears that ERA interim underestimates wind speed

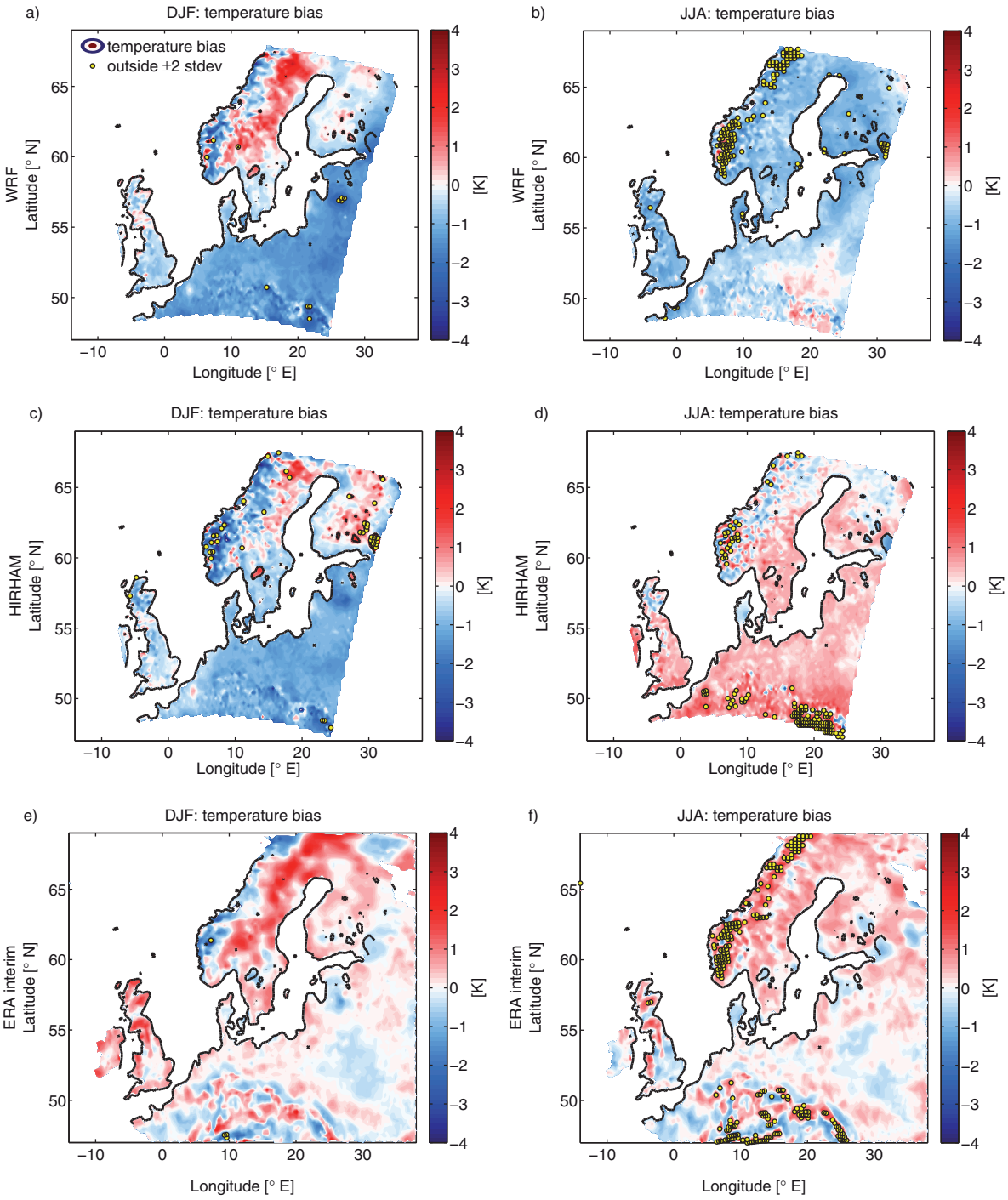

Fig. 2. Biases of seasonal temperature in K (simulation minus E-OBS data) in the WRF simulation for (a) winter and (b) summer season; (c, d) for the HIRHAM5 simulation; and (e, f) for ERA interim. Model data is re-projected bilinearly to the E-OBS 0.22° rotated grid. Yellow dots indicate grid points where the model biases lie outside an interval of ±2 standard error which is given within the E-OBS data set.

by 2–2.4 m s^{-1} between Scotland and the coast of western Norway (see Fig. 5e). For this region, both RCMs show a reduction of the wind speed bias by 1–2 m s^{-1} and an increase in frequency skill scores (not shown). This is within a region which is known for the mesoscale sensitivity to large-scale wind speeds particularly during winter time when low pressure systems impinge the Scandinavian peninsula, and air masses are accelerated

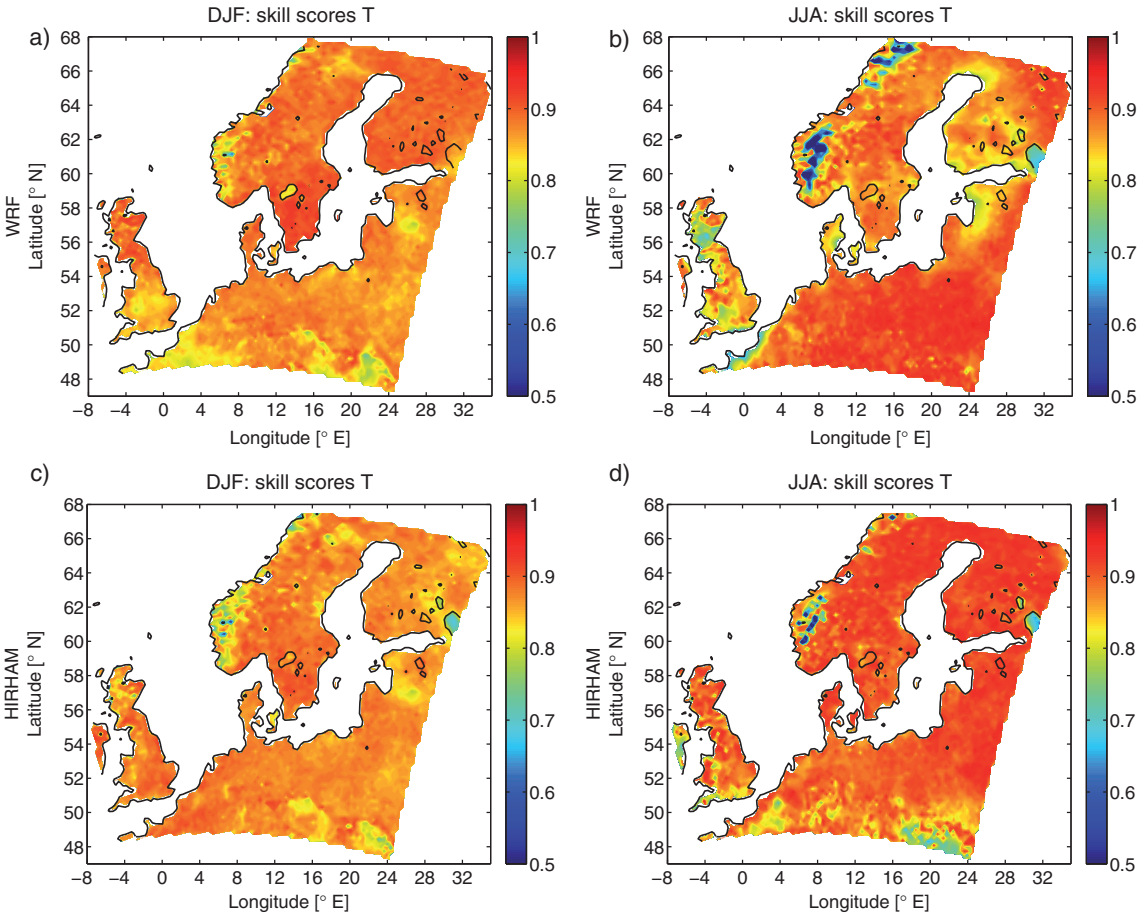

Fig. 3. Skill scores for daily mean temperature, T, for the WRF simulation for the seasons (a) winter and (b) summer; (c, d) as simulated in HIRHAM5. The skill score is dimensionless and ranges from 0 to 1, where 1 is a perfect match between the observed and modelled distributions. The colour bar ranges from 0.5 to 1 to make regional differences more visible.

along the southwest Norwegian coast (Barstad and Grønås, 2005).

4.3. *Precipitation*

Overall both models exhibit a wet bias of 50–100% (1–3 mm day^{-1}) in seasonal precipitation (see Fig. 6). This bias is mostly pronounced in winter. For example, ERA interim shows a wet bias over parts of Poland and Belarus which increases within both RCM downscalings. This is also reflected in the skill score maps (Fig. 7) as these regions show slightly lower skill scores ranging between 0.8 and 0.85, while the bulk of the study area shows $S_{score} \geq 0.85$. However, in summer the wet bias in simulated precipitation (Fig. 6) is less pronounced and frequency skill scores are generally higher in these regions compared to winter.

Considering seasonal wet-day precipitation on a local scale, ERA interim shows an underestimation in all four seasons over Bergen, Oslo and Copenhagen by 13–36% (Table 2). The RCM simulations show quite a large reduction in most cases of the negative bias and indicate a sign change in some seasons/locations.

Precipitation extremes can be caused by different types of weather patterns that occur predominantly in different seasons. During winter, most extreme precipitation is caused by advective systems, that is, low-pressure systems and storms that originate over the North Atlantic and impact the north European continent. In contrast, most summer precipitation extremes are caused by more localised convective systems. For example, in Copenhagen (see Fig. 8a and b), the most extreme precipitation with up to 70 mm day^{-1} occurs during summer when convective systems are more active. In Oslo, the difference in precipitation amounts is not as clear as for Copenhagen and in both winter and summer extreme precipitation ranges between 15 and 55 mm day^{-1}. However, in Bergen most extreme precipitation is caused by storms during fall and winter that impinge the Norwegian west coast causing extremes

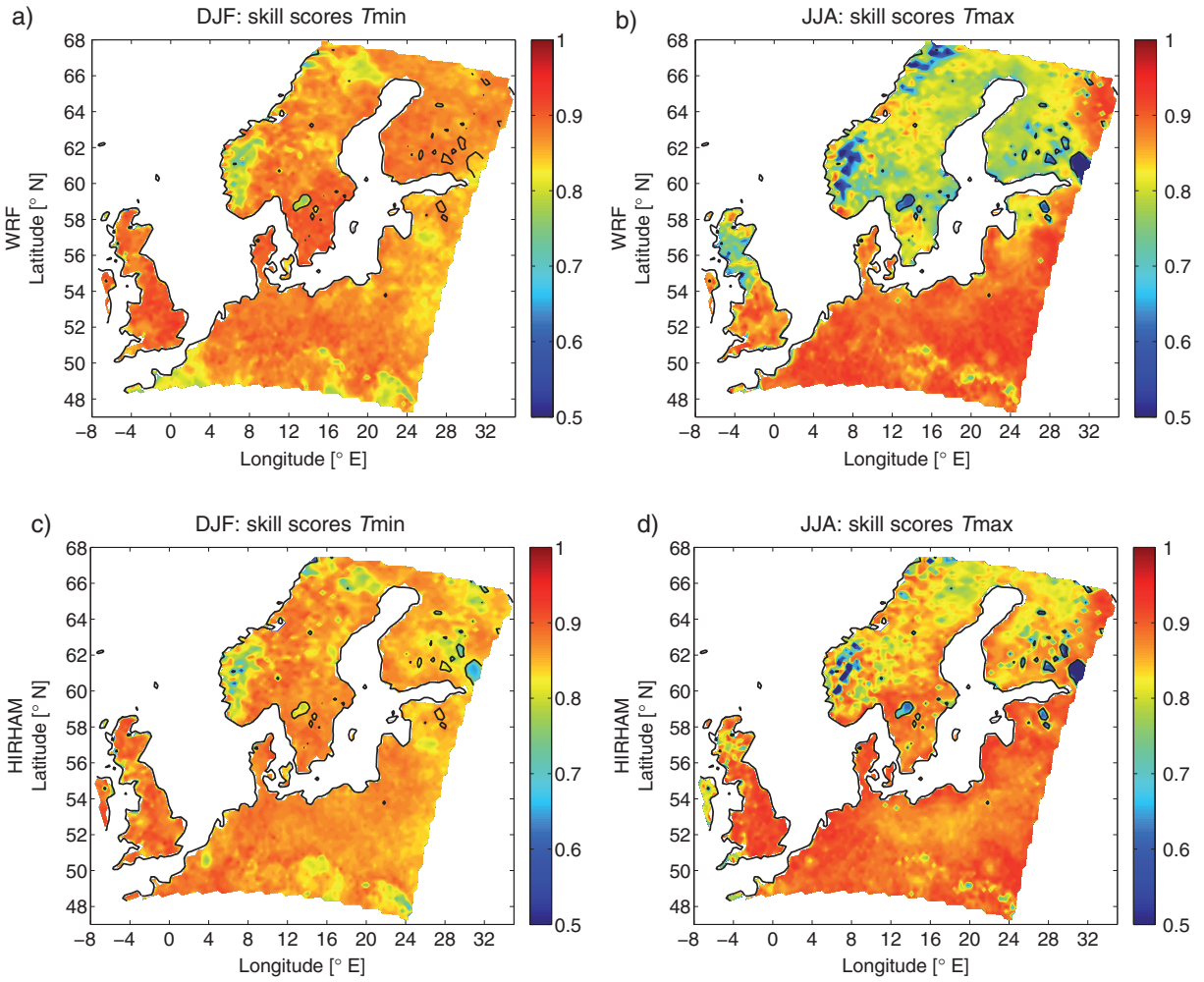

Fig. 4. As in Fig. 3 for extreme temperatures. (a) winter minimum temperature, *T*min, in WRF and (c) *T*min in HIRHAM5. (b) and (d) represent the skill scores in summer maximum temperatures, *T*max, in WRF and HIRHAM5, respectively.

of 100 mm day^{-1}. ERA interim considerably underestimates extreme precipitation in all locations in both seasons (blue line in Fig. 8). Both models either agree very well with the observations or lie above them (Fig. 8f for Bergen is an exception). Assuming a wind-induced underestimation of approximately 10–20% in the observations (indicated by a grey band in Fig. 8), this is a clear improvement compared to ERA interim.

As a further step to validate the models with respect to the need for both high temporal and spatial resolution in hydrological applications, we evaluated the spatio-temporal correlation of downscaled precipitation extremes (see Fig. 9). The sharp exponential decay in the 3-hourly observational correlation structure indicates that these events are highly localised, while this behaviour is not reflected within the ERA interim data. Just by visual comparison both RCM downscalings are much closer to the observational behaviour, suggesting that short duration extreme precipitation is well captured by both models. To quantify the differences of the correlation curves, the e-folding distances were calculated as suggested by Gregersen et al. (2013). The values are summarised in Table 3. Typically for shorter durations (3 hours) shorter correlation lengths are obtained; that is, extreme precipitation on a short time scale is very localised (<10 km) in reality. Both for subdaily and daily extreme precipitation, this behaviour is not represented at all in ERA interim with correlation differences beyond 100 km. However, both RCMs are much closer to a realistic behaviour with correlation differences of 30 km on a subdaily time scale and 40 km on a daily time scale. This is also an improvement compared to ENSEMBLES simulations on a 25 km grid where correlation differences of 50–80 km on a subdaily time scale were identified by Gregersen et al. (2013).

As a final step we compare the scaling properties of the non-central moments estimated from the precipitation

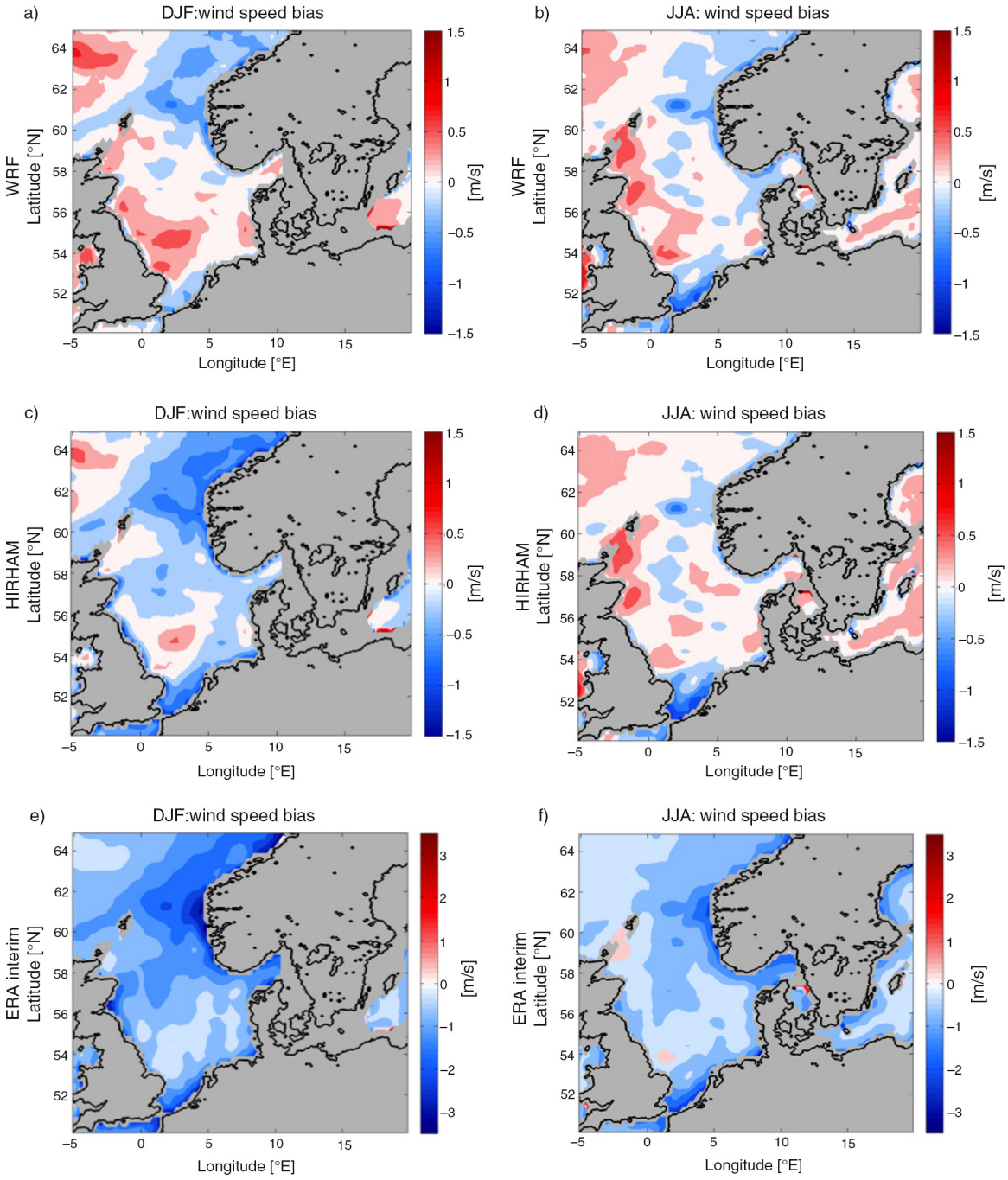

Fig. 5. Biases of wind speed in m s^{-1} (simulation minus Qscat) in (a) and (b) WRF; (c, d) HIRHAM; and (e, f) ERA interim. The winter season is shown in the left column and the summer season in the right column. Grey areas indicate no data.

observations at Landbohøjskolen in Copenhagen, the RCM simulations and ERA interim. Figure 10 shows the logarithm of the non-central moments ($log(Mn(q))$) estimated for each temporal aggregation for winter (DJF) and summer (JJA). The first moment ($q = 1$) is the mean precipitation, the second moment is equivalent to the variance. The third and fourth moments are considered high-order moments. They are equivalent to the skewness (a measure of the asymmetry) and kurtosis (a measure of peakedness) of the distribution. High-order moments are an indication of the extreme precipitation properties, higher values of these moments translate into higher extreme events. On the abscissa, $log(\lambda) = 0$ corresponds to a temporal aggregation of 24 hours and $log(\lambda) = -1.4$ corresponds to 1 hour,

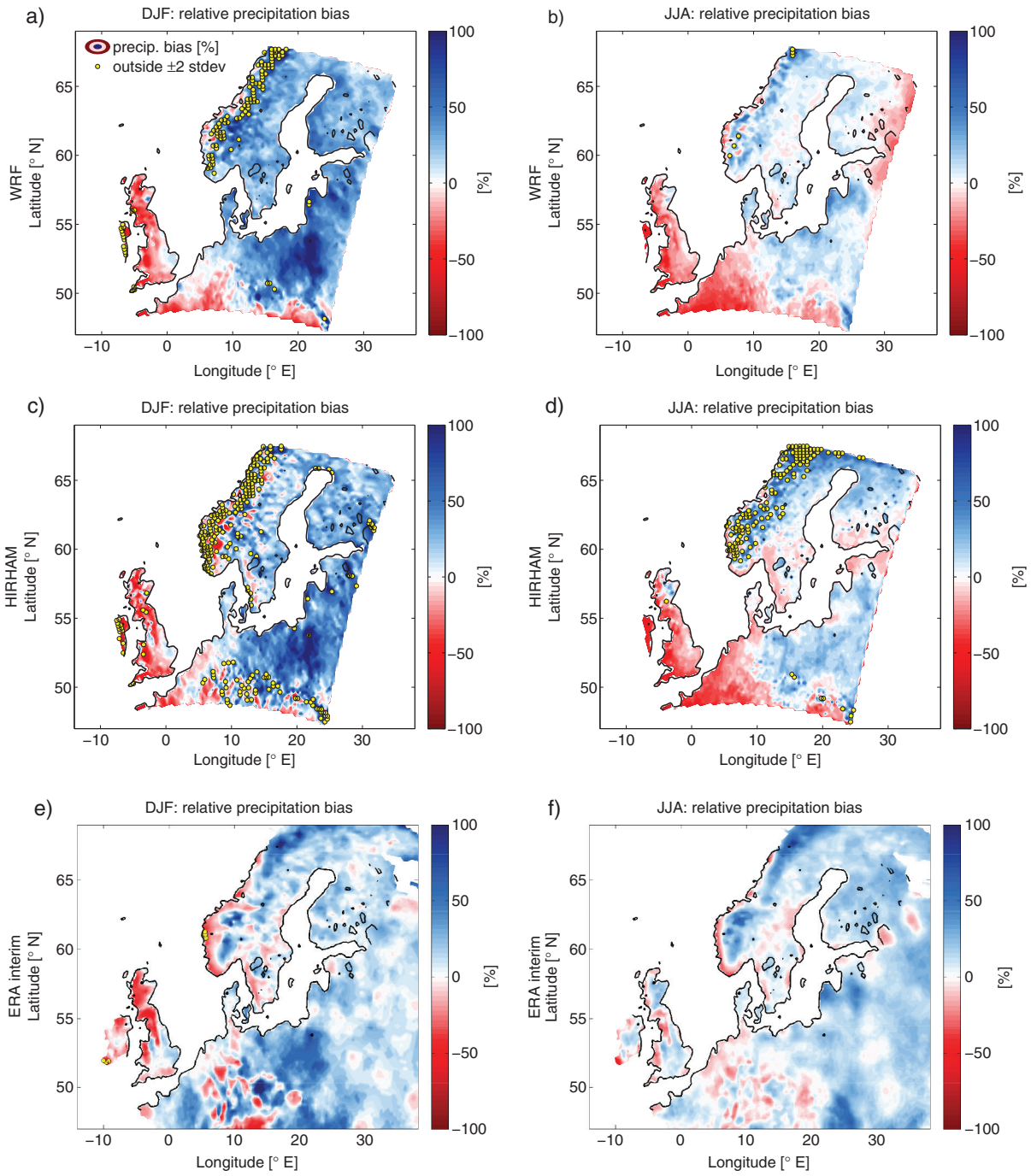

Fig. 6. Relative precipitation bias, $RPB = (\frac{RCM}{E-OBS} - 1) \cdot 100\%$ in the WRF simulation for (a) winter and (b) summer season; (c, d) for the HIRHAM5 simulation; and (e, f) for ERA interim. Yellow dots indicate grid points where the model biases lie outside an interval of ± 2 standard error which is given within the E-OBS data set. The absolute error ranges between ± 3 mm day^{-1}.

respectively. ERA interim is only available for temporal aggregations of 3–24 hours.

In winter, both RCMs and ERA interim overestimate the mean precipitation ($q = 1$) for all temporal aggregations but the overestimation is less pronounced in the reanalysis (blue line). For this season and for the second and high-order moments (i.e. $q = 2,3$ and 4), ERA interim shows an underestimation and the RCMs an overestimation; that is, ERA interim underestimates extreme precipitation, while the RCMs overestimate it. For all moments, ERA interim is

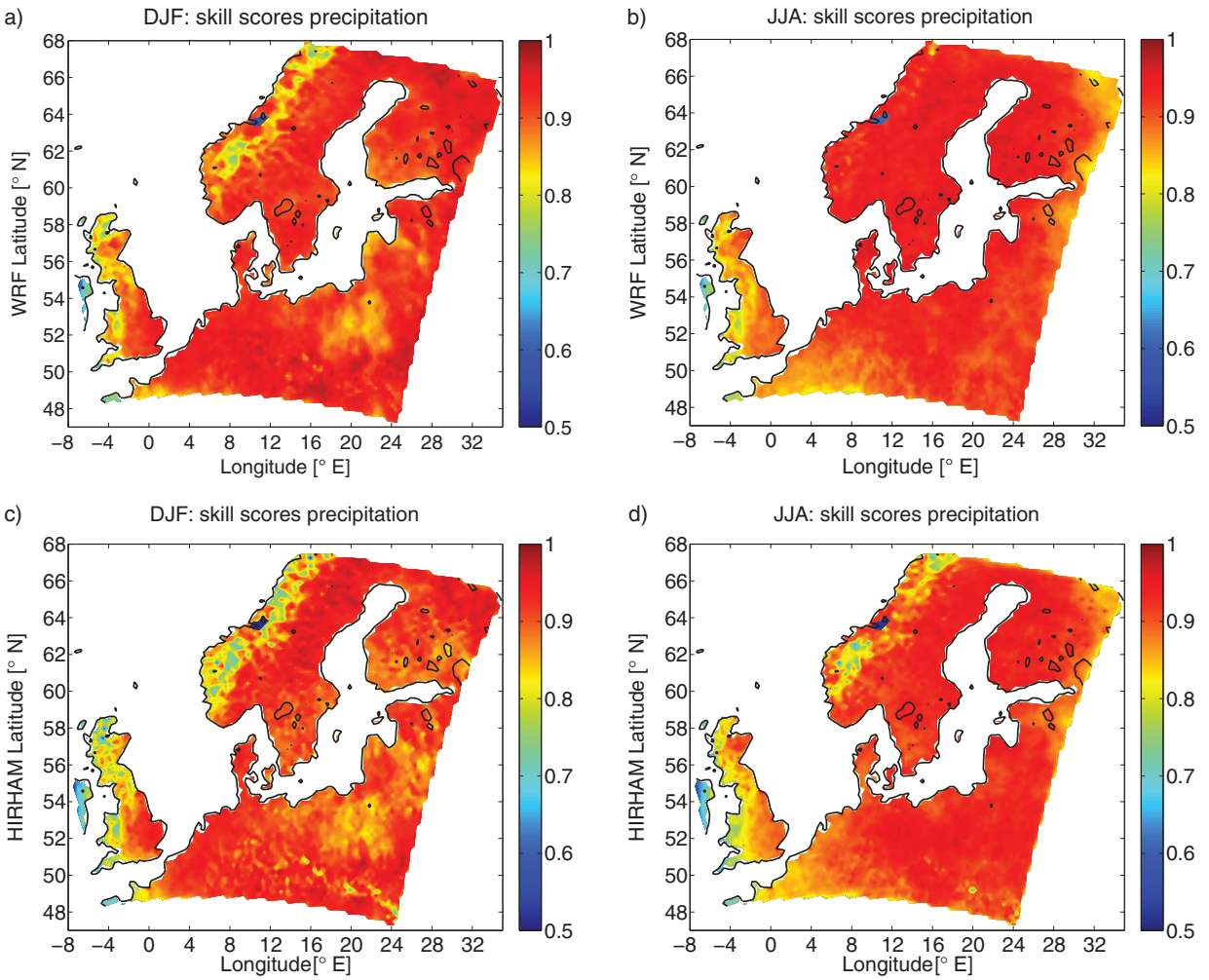

Fig. 7. As in Fig. 3 for daily mean precipitation amounts for the WRF simulation for the seasons (a) winter and (b) summer; c, d) as simulated in HIRHAM5.

closer to the observations than the RCMs for large durations (12 and 24 hours). On the other hand, for durations of 3 and 6 hours and high order moments ($q = 3$ and 4), HIRHAM is closer to the observations than WRF and ERA interim. The slopes of the linear regressions estimated for the RCMs and ERA interim for all the moments are steeper than in the observations. This indicates that the overestimation of precipitation in the RCMs is higher at 24 hours than at 1 hour, while the opposite occurs for ERA interim. In summer, both RCM simulations are closer to the observational statistical moments than for winter. For this season, WRF (red line) overestimates mean precipitation, while HIRHAM (green line) and ERA interim slightly underestimate it. In the second and higher order moments, ERA interim clearly exhibits an underestimation for all temporal aggregations. For these moments ($q = 2,3$ and 4), both RCMs are considerably closer to the observations than ERA interim. HIRHAM slightly overestimates extreme precipitation (overestimation of moments of order 3 and 4), while WRF shows a small underestimation. For these moments ($q = 3$ and 4) and all durations, the values obtained from WRF are closer to the observations than the values obtained for HIRHAM. It must also be noted that for all moments HIRHAM shows a similar performance for all temporal aggregations, while the performance of WRF enhances for larger durations. These results show that WRF is closer to the observation when looking at the value of the moments but that HIRHAM is closer to the observations when comparing the slopes of the linear regressions. In summary, both RCMs show a clear improvement in the representation of summer extreme precipitation compared to ERA interim, but in winter the results depend on the temporal aggregation. As expected, in both seasons larger biases occur in the magnitude of the moments, and in the slope of the linear regressions for high-order moments.

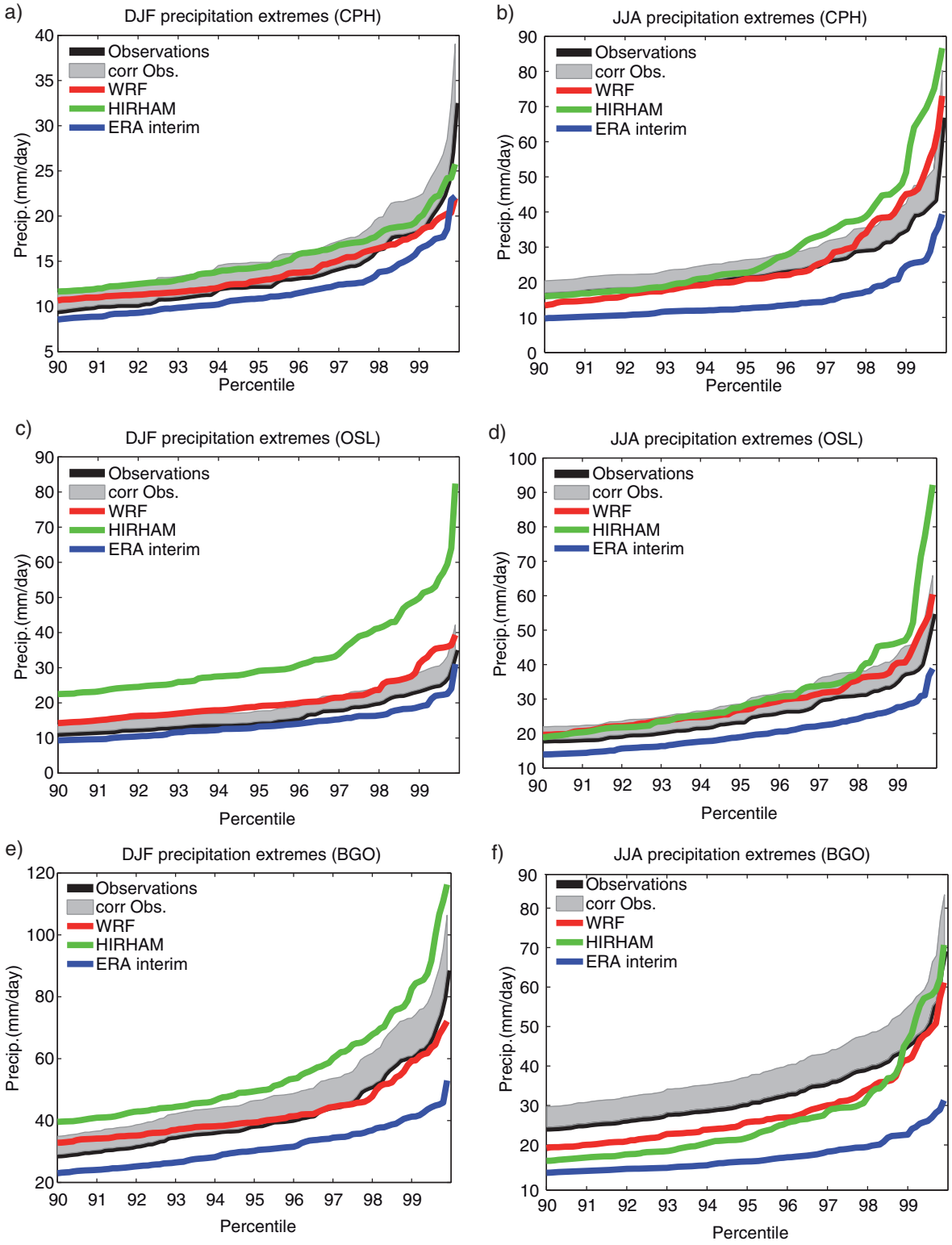

Fig. 8. 90–99.9 percentiles for extreme precipitation in mm day^{-1} for (a) and (b) Copenhagen; (c, d) Oslo; and (e, f) Bergen. Corresponding model data was retrieved with the nearest-neighbour method for the single locations. The subfigures in the left column represent wintertime (DJF) extreme precipitation. In the right column, summertime (JJA) extreme precipitation is shown. An assumed observational undercatch of 20% is illustrated with a grey band.

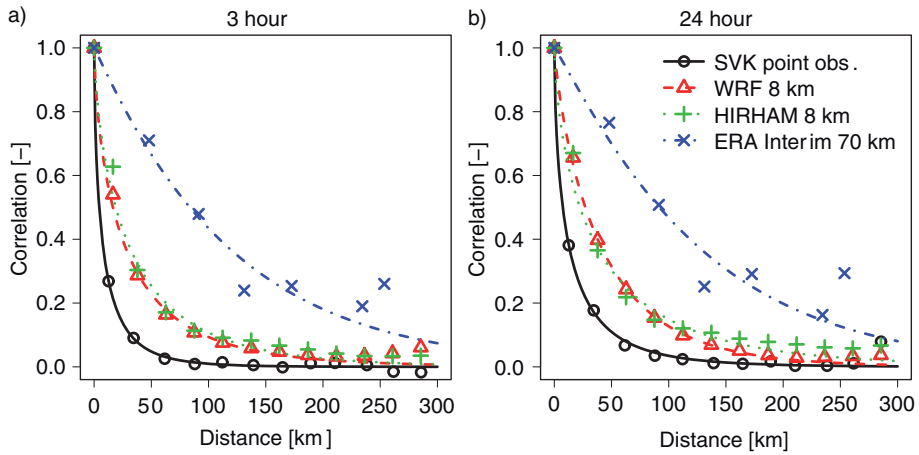

Fig. 9. Spatio-temporal correlation structure of observed (SVK), ERA interim (70 km) and downscaled (8 km) mean intensities of extreme precipitation for 3 hour (a) and 24 hour (b) duration. To highlight the tendencies, an exponential function is used for fitting by using the least-square method.

Figure 11 shows $\tau(q)$ (the negative value of the slopes in Fig. 10). In this figure, overestimation (underestimation) of τ indicates that the models overestimate (underestimate) the importance of precipitation at short durations. For example, in the case of $q=2$, an overestimation of τ means that the comparison of the RCM with the observations shows that the variance at 1 hour resolution is too large in relation to the variance at 24 hours. In winter, the RCMs and ERA interim underestimate the value of τ found for the observations for $q>1$. A smaller bias is obtained for HIRHAM and ERA interim. This indicates that both the RCMs and ERA interim underestimate the importance of short duration precipitation; that is, precipitation at long durations is more relevant than at short durations. In summer, HIRHAM shows the same τ as the observations for $q<3$, while it slightly overestimates τ for $q\geq 3$. The overestimation of τ for high-order moments shows that this model overestimates more extreme precipitation at short duration compared to long duration precipitation. ERA interim and WRF underestimate τ for all moments $q>1$. This indicates that they underestimate the importance of precipitation at short durations more compared to long duration.

Table 3. Estimated e-folding distances in km of extreme precipitation for the duration of 3 hours and 24 hours

	3 hours	24 hours
SVK	8	13
WRF	28	42
HIRHAM	32	32
ERA interim	119	128

As in Gregersen et al. (2013), the estimates are derived from the fitted exponential models shown in Fig. 9.

5. Conclusion and discussion

This paper introduces a set of two new high-resolution ($\sim$8 km) RCM simulations performed with WRF and HIRHAM5 over Scandinavia and the surrounding seas. The study assesses how well the two RCMs simulate temperature, wind speed and precipitation in the study area. The motivation for this study was whether added value can be identified using high-resolution RCMs compared to the lower resolution ERA interim data product. The term 'added value' is used in the sense of whether higher resolution models simulate critical aspects of the observed climate in a more realistic way compared to lower resolution data products such as ERA interim.

Seasonal surface temperature and precipitation over land, and surface wind speed over the North Sea were evaluated for bias and skill. Seasonal temperature and precipitation biases were also examined for selected urban locations. Daily extremes of precipitation were evaluated by comparing the upper decile of the models, observations and reanalysis. To evaluate if the models are fit for purpose, for example, hydrology applications, the spatial structure and statistical moments of subdaily precipitation was investigated at selected locations with point-scale observations.

In summary, biases of seasonal temperature and precipitation in both models are mostly within the observational uncertainty, and when comparing them to ERA interim, a direct improvement is not evident. However, this was to be expected due to temporal smoothing when considering seasonal means. ERA interim and the RCMs capture the shape of the daily temperature and precipitation distributions (seasonal skill scores). Both models perform well in the representation of seasonal wind speeds over the North Sea especially in the region west of the Norwegian southwest

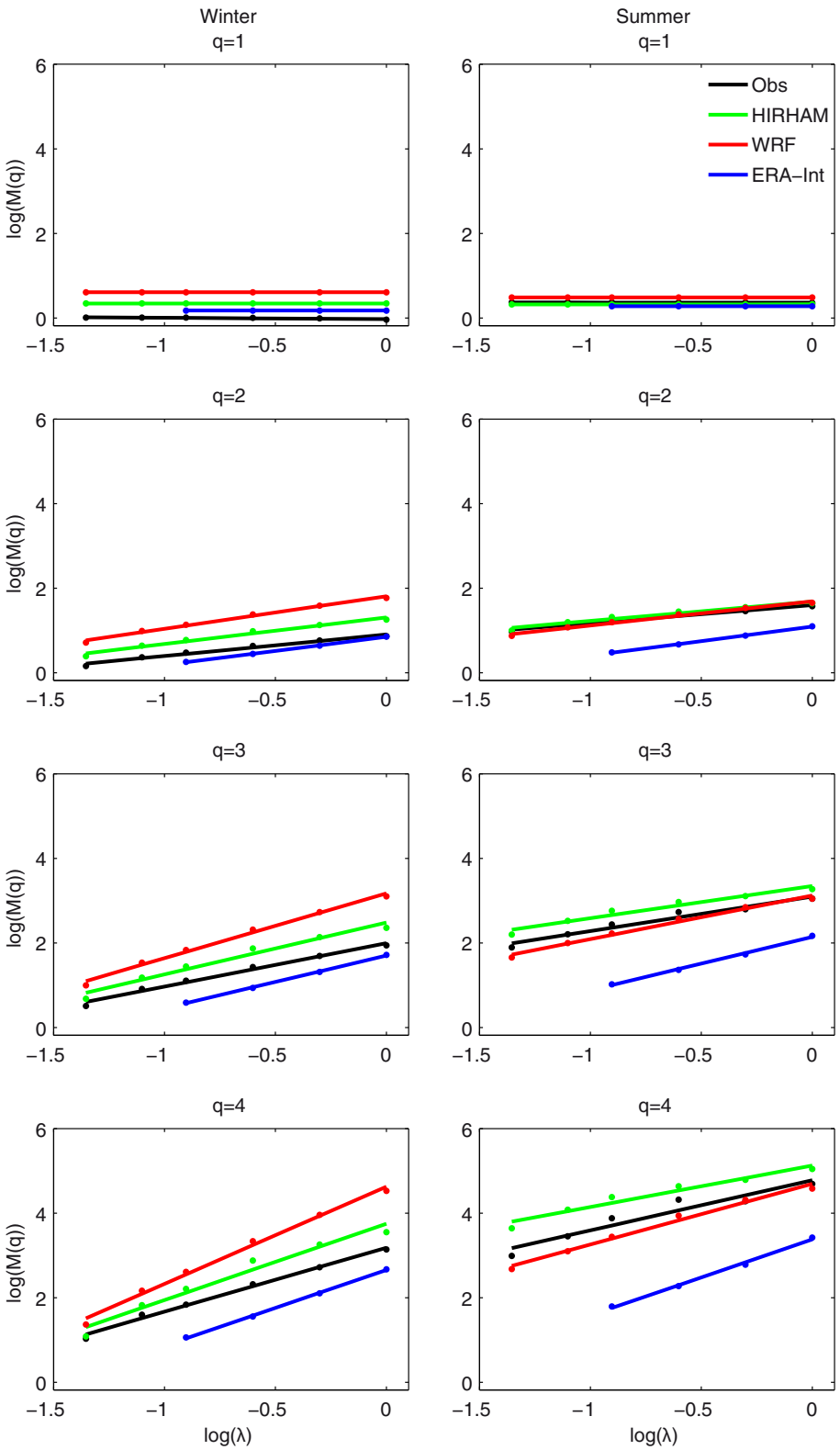

Fig. 10. Moment scaling relationships for the observed and simulated precipitation in Copenhagen during winter (left) and summer (right). $q = 1$ mean; $q = 2$ standard deviation; $q = 3$ skewness and $q = 4$ kurtosis. The abscissa represents the different temporal aggregations.

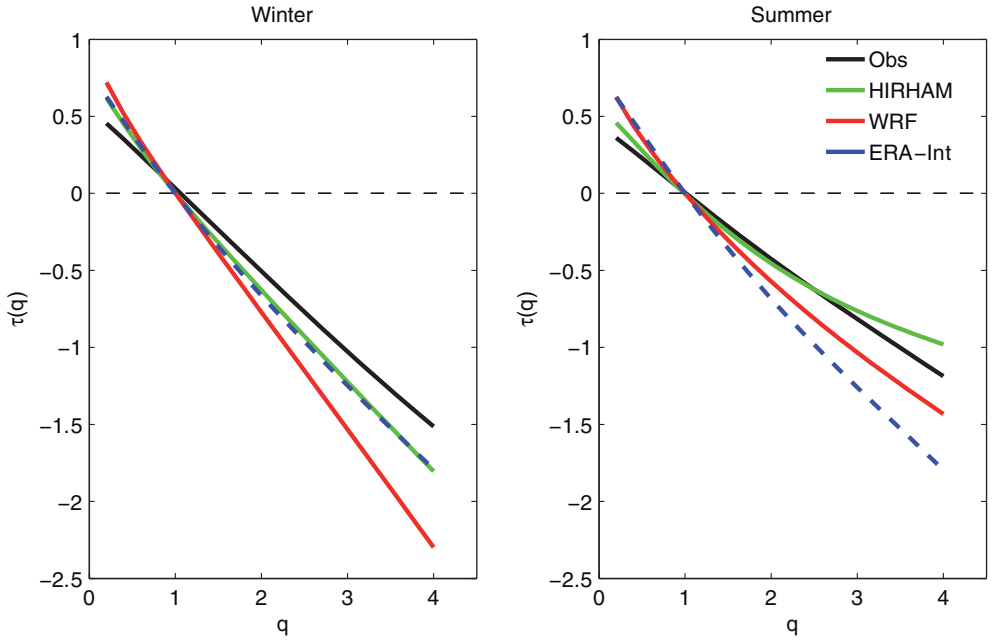

Fig. 11. Summary of Fig. 10 with the different slopes τ as a function of the statistical moments q.

coast. For this area, added value compared to ERA interim both in the representation of seasonal means and frequency skill scores is found; that is, wind speed biases in the RCMs are reduced and skill scores are increased. This improvement may be a direct consequence of a better representation of dynamic mesoscale features due to the higher horizontal resolution within the RCM simulations.

Considering wet-day precipitation, for the selected locations, Bergen, Oslo and Copenhagen, we find that in the reanalysis it rains too often but overall too little. Both RCMs capture the timing of precipitation especially during summer more realistically. Clearly, added value is identified in the spatio-temporal representation of extreme precipitation for Denmark on daily to subdaily scale. In addition to better capturing the magnitude of extreme precipitation, the models are also able to capture the highly localised spatial structure of extreme precipitation events. The analysis of statistical moments of precipitation for the location of Copenhagen yield that the models show a clear improvement (added value) compared to ERA interim during summer. For the city of Copenhagen, this is an important result since summer time extreme precipitation (thunderstorms and cloud bursts) is a challenge for the city sewage water systems to catch large water masses during a short time. One example was the cloud burst on 2 July 2011 that caused substantial building damages resulting in insurance claims of approximately 600 million Euros (Kaspersen, 2013). Under the assumption of a warmer and wetter climate in mid-latitudes, convective extreme precipitation may increase and the design of infrastructures has to be adapted accordingly. Within the RiskChange project, both models are currently run to dynamically downscale global climate model projections for the near-future period of 2021–2050 and the far-future period 2071–2100 under the assumption of climate change with the representative concentration pathways rcp4.5 and rcp8.5. This will enable projections of changes in extreme precipitation at high temporal and spatial resolution and contribute to a new data repository for adaptation purposes. This will be the subject of a separate paper.

Finally, we note that both models, and their computationally very expensive set up (8-km grid, hourly output), show a clear improvement compared to lower resolution reanalysis data, provided one is interested in subdaily timescales and a more accurate spatial structure of extreme precipitation events. Hence, the models' expense needs to be weighed against the purpose they are intended for.

6. Acknowledgements

This work was carried out within the RiskChange project which is supported by the Danish Council for Strategic Research, Contract 10-093894 and DNV-GL, project number 804836. We acknowledge the E-OBS data set from the EU-FP6 project ENSEMBLES (http://ensembles-eu.metoffice.com) and the data providers in the ECA&D project (http://www.ecad.eu). Super-computing resources on a Cray XE6m-200 computer at Parallab at the University of Bergen have been made available by the Norwegian Research Council through the NOTUR project.

References

Arnbjerg-Nielsen, K., Willems, P., Olsson, J., Beecham, S., Pathirana, A. and co-authors. 2013. Impacts of climate change on rainfall extremes and urban drainage systems: a review. *Water Sci. Technol.* **68**(1), 16–28.

Barstad, I. and Caroletti, G. 2013. Orographic precipitation across an island in southern Norway: model evaluation of time-step precipitation. *Q. J. Roy. Meteorol. Soc.* **139**(675), 1555–1565.

Barstad, I. and Grønås, S. 2005. Southwesterly flows over southern Norway – mesoscale sensitivity to large-scale wind direction and speed. *Tellus A*. **57**(2), 136–152.

Barstad, I., Sorteberg, A., Flatøy, F. and Déqué, M. 2009. Precipitation, temperature and wind in Norway: dynamical downscaling of ERA40. *Clim. Dynam.* **33**(6), 769–776.

Barstad, I., Sorteberg, A. and Mesquita, M. 2012. Present and future offshore wind power potential in northern Europe based on downscaled global climate runs with adjusted SST and sea ice cover. *Renew. Energy*. **44**, 398–405.

Bates, B., Kundzewicz, Z., Wu, S. and Palutikof, J. (eds.). 2008. *Climate Change and Water. Technical paper VI*. IPCC Secretariat, Geneva.

Bourassa, M. A., Legler, D. M., O'Brien, J. J. and Smith, S. R. 2003. Sea Winds validation with research vessels. *J. Geophys. Res.* **108**, 3019.

Burlando, P. and Rosso, R. 1996. Scaling and multiscaling models of depth-duration-frequency curves for storm precipitation. *J. Hydrol.* **187**, 45–64.

Burton, A., Kilsby, C. G., Fowler, H. J., Cowpertwait, P. S. P. and O'Connell, P. E. 2008. RainSim: a spatial-temporal stochastic rainfall modelling system. *Environ. Model. Softw.* **23**, 1356–1369.

Christensen, J. H. and Christensen, O. B. 2003. Climate modelling: severe summertime flooding in Europe. *Nature*. **421**(6925), 805–806.

Christensen, J. H. and Christensen, O. B. 2007. A summary of the PRUDENCE model projections of changes in European climate by the end of this century. *Clim. Change*. **81**(1), 7–30.

Christensen, J. H., Kjellström, E., Giorgi, F., Lenderink, G. and Rummukainen, M. 2010. Weight assignment in regional climate models. *Clim. Res.* **44**(2–3), 179–194.

Christensen, O. B., Drews, M., Christensen, J. H., Dethloff, K., Ketelsen, K. and co-authors. 2006. *The HIRHAM Regional Climate Model Version 5 (β)*. Danish Meteorological Institute Technical Report, Copenhagen, DK, pp. 6–17.

Collins, W. D., Rasch, P. J., Boville, B. A., Hack, J. J., McCaa, J. R. and co-authors. 2004. *Description of the NCAR Community Atmosphere Model (CAM 3.0)*. NCAR Tech. Note NCAR/TN-464+ STR, 214 pp.

Dee, D., Uppala, S., Simmons, A., Berrisford, P., Poli, P. and co-authors. 2011. The ERA-Interim reanalysis: configuration and performance of the data assimilation system. *Q. J. Roy. Meteorol. Soc.* **137**(656), 553–597.

Ek, M., Mitchell, K., Lin, Y., Rogers, E., Grunmann, P. and co-authors. 2003. Implementation of Noah land surface model advances in the National Centers for Environmental Prediction operational mesoscale Eta model. *J. Geophys. Res.* **108**(D22), 8851.

EU. 2011. Commission Recommendation of 21.10.2011 on the research joint programming initiative. January 'Connecting Climate Knowledge for Europe', 21.10.2011. C(2011) 7410 final, European Commission, Brussels. Online at: http://ec.europa.eu/research/participants/portal/doc/call/fp7/fp7-jprog'-2012-rtd/31942-commission_recommendation_c(2011)7410_final_en.pdf

Giorgetta, M. and Wild, M. 1995. *The Water Vapour Continuum and Its Representation in ECHAM4*. Technical Report 38, Max Planck Institut für Meteorologie, Hamburg, Germany.

Gregersen, I., Sørup, H., Madsen, H., Rosbjerg, D., Mikkelsen, P. and co-authors. 2013. Assessing future climatic changes of rainfall extremes at small spatio-temporal scales. *Clim. Change*. **8**(4), 783–797.

Gupta, V. and Waymire, E. 1993. A statistical analysis of mesoscale rainfall as a random cascade. *J. Appl. Meteorol.* **32**, 251–267.

Hanson, C., Palutikof, J., Livermore, M., Barring, L., Bindi, M. and co-authors. 2007. Modelling the impact of climate extremes: an overview of the MICE project. *Clim. Change*. **81**(1), 163–177.

Haylock, M., Hofstra, N., Klein Tank, A., Klok, E., Jones, P. and co-authors. 2008. A European daily high-resolution gridded data set of surface temperature and precipitation. *J. Geophys. Res. (Atmospheres)*. **113**(D20119), 1–12.

IPCC. 2012. Summary for policymakers. In: *Managing the Risks of Extreme Events and Disasters to Advance Climate Change Adaptation. A Special Report of Working Groups I and II of the Intergovernmental Panel on Climate Change*. (eds. C. B. Field, V. Barros, T. F. Stocker, D. Qin, and D. J. Dokken et al.), Cambridge University Press, Cambridge, UK, pp. 1–19.

Jacob, D., Bärring, L., Christensen, O. B., Christensen, J. H., de Castro, M. and co-authors. 2007. An inter-comparison of regional climate models for Europe: model performance in present-day climate. *Clim. Change*. **81**(1), 31–52.

Janjić, Z. 2002. Nonsingular implementation of the Mellor–Yamada level 2.5 scheme in the NCEP Meso model. *NCEP Office Note*. **437**, 61.

Kaspersen, P. 2013. Flood risk from extreme precipitation in Copenhagen – modelling results. *European Climate Change Adaptation Conference*, Hamburg, March 18–20, 2013. Online at: http://www.eccaconf.eu/presentations/PDF/ECCA2013-1a-6_10_4-Kaspersen.pdf

Kjellström, E. and Giorgi, F. 2010. Introduction. *Clim. Res.* **44**, 117–119.

Klein Tank, A., Wijngaard, J., Können, G., Böhm, R., Demarée, G. and co-authors. 2002. Daily dataset of 20th-century surface air temperature and precipitation series for the European Climate Assessment. *Int. J. Climatol.* **22**(12), 1441–1453.

Lohmann, U. and Roeckner, E. 1996. Design and performance of a new cloud microphysics scheme developed for the ECHAM4 general circulation model. *Clim. Dynam.* **12**, 557–572.

Louis, J. 1979. A parametric model of vertical eddy fluxes in the atmosphere. *Boundary Layer Meteorol.* **17**, 187–202.

Lungu, T. E. 2001. *QuikSCAT Science Data Product User's Manual: Overview and Geophysical Data Products*. Technical Report V2.2, JPL D-18053, Jet Propulsion Laboratory, Pasadena, CA, 95 pp.

Madsen, H., Mikkelsen, P., Rosbjerg, D. and Harremoes, P. 2002. Regional estimation of rainfall intensity-duration-frequency curves using generalized least squares regression of partial duration series statistics. *Water Resour. Res.* **38**, 1239.

Maraun, D., Wetterhall, F., Ireson, A. M., Chandler, R. E., Kendon, E. J. and co-authors. 2010. Precipitation downscaling under climate change. Recent developments to bridge the gap between dynamical models and the end user. *Rev. Geophys.* **48**, RG3003.

Mikkelsen, P., Madsen, H., Rosbjerg, D. and Harremoes, P. 1996. Properties of extreme point rainfall III: identification of spatial inter-site correlation structure. *Atmos. Res.* **40**(1), 77–98.

Molnar, P. and Burlando, P. 2005. Preservation of rainfall properties in stochastic disaggregation by a simple random cascade model. *Atmos. Res.* **77**, 137–151.

Morcrette, J.-J. 1991. Radiation and cloud radiative properties in the ECMWF forecasting system. *J. Geophys. Res.* **96**(D5), 9121–9132.

Onof, C. and Arnbjerg-Nielsen, K. 2009. Quantification of anticipated future changes in high resolution design rainfall for urban areas. *Atmos. Res.* **92**, 350–363.

Over, T. and Gupta, V. 1996. A space–time theory of mesoscale rainfall using random cascades. *J. Geophys. Res.* **101**(D21), 26319–26331.

Perkins, S., Pitman, A., Holbrook, N. and McAneney, J. 2007. Evaluation of the AR4 climate models' simulated daily maximum temperature, minimum temperature, and precipitation over Australia using probability density functions. *J. Clim.* **20**(17), 4356–4376.

Ricciardulli, L. and Wentz, F. 2011. *Reprocessed QuikSCAT (V04) Wind Vectors with Ku-2011 Geophysical Model Function*. RSS Technical report number 043011, Remote Sensing Systems, Santa Rosa, CA, 8 pp.

Rummukainen, M. 2010. State-of-the-art with regional climate models. *Wiley Interdiscip. Rev. Clim. Change*. **1**(1), 82–96.

Skamarock, W., Klemp, J., Dudhia, J., Gill, D. and Barker, D. 2005. *A Description of the Advanced Research WRF version 3*. NCAR Tech. Note NCAR/TN-475+ STR, 113 pp.

Soares, P. M. M., Cardoso, R. M., Miranda, P. M. A., de Medeiros, J., Belo-Pereira, M. and co-authors. 2012. WRF high resolution dynamical downscaling of ERA-Interim for Portugal. *Clim. Dynam.* **39**(9–10), 2497–2522.

Stohl, A., Forster, C. and Sodemann, H. 2008. Remote sources of water vapor forming precipitation on the Norwegian west coast at 60°N-a tale of hurricanes and an atmospheric river. *J. Geophys. Res.* **113**(D05102), 1–13.

Sunyer, M., Sørup, H., Madsen, H., Rosbjerg, D., Christensen, O. and co-authors. 2013. On the importance of observational data properties when assessing regional climate model performance of extreme precipitation. Hydrol. *Earth System Sci.* **17**, 4323–4337.

Thompson, G., Field, P. R., Rasmussen, R. M. and Hall, W. D. 2008. Explicit forecasts of winter precipitation using an improved bulk microphysics scheme. Part II: Implementation of a new snow parameterization. *Mon. Weather Rev.* **136**(12), 5095–5115.

Tiedtke, M. 1989. A comprehensive mass flux scheme for cumulus parameterization in large-scale models. *Mon. Weather Rev.* **117**(8), 1779–1800.

Uppala, S., Kållberg, P., Simmons, A., Andrae, U., Da Costa Bechtold, V. and co-authors. 2005. The ERA-40 re-analysis. *Q. J. Roy. Meteorol. Soc.* **131**(612), 2961–3012.

van Deelen, K., Driessen, P., Swart, R., Joussaume, S., Sorvari, S. and co-authors. 2011. *Joint Programming Initiative Connecting Climate Change Knowledge for Europe (JPI Climate)*. Technical report, Strategic Research Agenda. Online at: http://www.jpi-climate.eu/publications/documents/10826597/JPI-Climate-Strategic-Research-Agenda

van der Linden, P. and Mitchell, J. E. 2009. *ENSEMBLES: Climate Change and its Impacts: Summary of Research and Results from the ENSEMBLES Project*. Technical Report, Met Office Hadley Centre, Exeter, UK, 160 pp.

Warner, T. T. 2011. *Numerical Weather and Climate Prediction*, Vol. 526. Cambridge University Press, Cambridge.

Wilby, R. and Dessai, S. 2010. Robust adaptation to climate change. *Weather*. **65**(7), 180–185.

Wilby, R. L. and Harris, I. 2006. A framework for assessing uncertainties in climate change impacts: low-flow scenarios for the River Thames, UK. *Water Resour. Res.* **42**, W02419.

Willems, P. and Vrac, M. 2011. Statistical precipitation downscaling for small-scale hydrological impact investigations of climate change. *J. Hydrol.* **402**, 193–205.

Zhang, C., Wang, Y. and Hamilton, K. 2011. Improved representation of boundary layer clouds over the Southeast Pacific in ARW-WRF using a modified Tiedtke Cumulus Parameterization Scheme. *Mon. Weather Rev.* **139**(11), 3489–3513.